The structure of molten CuCl: reverse Monte Carlo modeling with high-energy X-ray diffraction data and molecular dynamics of a polarizable ion model

Olga Alcaraz,[1] *Joaquim Trullàs,*[1] *Shuta Tahara,*[2] *Yukinobu Kawakita,*[3] and *Shin'ichi Takeda*[4]

[1]Departament de Física i Enginyeria Nuclear, Universitat Politècnica de Catalunya, Campus Nord UPC B4-B5, 08034 Barcelona, Spain.

[2]Department of Physics and Earth Sciences, Faculty of Science, University of the Ryukyus, Okinawa 903-0213, Japan.

[3]J-PARC Center, Japan Atomic Energy Agency (JAEA), Ibaraki 319-1195, Japan.

[4]Department of Physics, Faculty of Sciences, Kyushu University, Fukuoka 819-0395, Japan.

* Corresponding author. E-mail: quim.trullas@upc.edu

PACS numbers: 61.20.Ja, 61.20.Qg, 61.05.cp

The results of the structural properties of molten copper chloride are reported from high-energy X-ray diffraction measurements, reverse Monte Carlo modeling method and molecular dynamics simulations using a polarizable ion model. The simulated X-ray structure factor reproduces all trends observed experimentally, in particular the shoulder at around 1 $Å^{-1}$ related to intermediate range ordering, as well as the partial copper-copper correlations from the reverse Monte Carlo modeling, which cannot be reproduced by using a simple rigid ion model. It is shown that the shoulder comes from intermediate range copper-copper correlations caused by the polarized chlorides.

I. INTRODUCTION

The structure of molten copper chloride has been extensively studied since Page and Mika[1] reported in 1971 the pioneering analysis of neutron diffraction (ND) data obtained using isotope substitution to separate the three partial structure factors, $S_{ab}(k)$, and then derive the corresponding radial distribution functions, $g_{ab}(r)$. Their essential results were later confirmed by Eisenberg et al.,[2] who repeated the ND measurements and improved the corresponding analysis. The most significant result is the absence of a marked structure in the Cu–Cu correlations, with a deep penetration of Cu cations into the first coordination shell of anions around a given cation. Using the reverse Monte Carlo (RMC) method of structural modeling,[3] McGreevy and Pusztai[4] reanalyzed the NS data of Eisenberg et al.[2] and obtained a $g_{\mathrm{CuCu}}(r)$ with the first peak slightly higher than in the previous analyses, but also much lower than that for $g_{\mathrm{ClCl}}(r)$. This result is quite different from that found for molten alkali halides,[5,6] where the structure of the cations and the anions are similar, as was shown by Woodkcok,[7] also in 1971, from the first molecular dynamics (MD) simulation of a binary ionic liquid, and later from ND experiments employing isotope substitution.[8]

The structure factor $S_{\mathrm{N}}(k)$ from ND measurements for the natural composition of molten CuCl, CuBr and CuI, i.e., without isotopic substitution, was also measured by Shirakawa et al.[9] The most salient result is the clear prepeak at around 1 $\mathrm{Å}^{-1}$ in the $S_{\mathrm{N}}(k)$ of CuI, which becomes much lower in CuBr, and there is a shoulder in CuCl. These are both signs of intermediate range ordering at scales that are longer than the distance between neighboring ions. It is worth noting that the $S_{\mathrm{N}}(k)$ for molten AgI also presents a small maximum at around 1 $\mathrm{Å}^{-1}$.[10] More recently, ND experiments by Drewit et al.[11] for molten CuI and CuCl exhibit the same main trends as those by Shirakawa et al. However, while their results for CuI also present a clear prepeak, for the CuCl do not show any trace of shoulder, nor do those by Page and Mika, nor those by Eisenberg et al. for the natural composition. This discrepancy is one of the reasons that prompted us to carry out high energy X-ray diffraction (HEXRD) measurements of the Faber-Ziman structure factor $A_{\mathrm{X}}(k)$ reported in this work.

In order to explain the featureless cation-cation structure of molten CuCl, Eisenberg at al.[2] pointed out that the weakness of the ionicity combined with the small relative size of copper ions seems to favor the short distance between them. On the other hand, Howe et al.[12] noted the similarity between the structure of molten CuCl and that of solid AgI in the high temperature superionic α-phase (α-AgI), i.e. that at which the ionic conductivity is about 1 $(\Omega cm)^{-1}$, the same order as in molten state. In addition, Ginoza et al.[13] suggested that a featureless cation-cation structure could be present in other salts that melt from a superionic phase such as α-CuBr, α-CuI and α-AgI,[14,15]. This prediction was confirmed later by Allen and Howe[16] for CuBr, and by Waseda et al.[17] for CuI. Vashishta and Rahman[18,19] simulated the superionic behavior of the α-AgI and α-CuI using rigid ion pair potentials with the following three characteristics. i) The absolute value of effective charges is lower than e (the fundamental charge) to take into account the incomplete ionization of the ions (and, to some extent, the effect of covalent interactions). ii) The anionic radius is approximately double the cationic one. iii) The anionic polarizability is to some extent taken into account with effective pairwise monopole-induced dipole interactions. From now on, we will denote these potentials as VR. Moreover, Parrinello et al.[20] simulated the $\beta \rightarrow \alpha$ transition of AgI using the VR potential with a refined parameterization. The specific VR potentials of Parrinello el al. have been widely used to study solid AgI,[21,] and MD simulations of solid CuI have also been carried out by using the original VR potentials.[22]

All the above ideas prompted Stafford et al. [23,24] to carry out theoretical calculations of $S_{ab}(k)$ and $g_{ab}(r)$ within the hypernetted chain (HNC) approximation for molten AgI, CuI, CuBr, and CuCl using VR potentials. Their results turned out to qualitatively agree with the ND data of Takahashi et al. [25] for AgI, and those of Eisenberg et al.[2] for CuCl, despite some differences in the quantitative sense. Furthermore, MD simulations using the same potentials suggested that these molten salts retain the superionic character of the α-phase.[26] However, the calculated $S_N(k)$ for molten AgI fails to reproduce the almost featureless broad main peak, as well as the prepeak that appears at around 1 $Å^{-1}$,[27] exhibited by ND data.[10] In addition, the VR potentials also fail to reproduce the clear sharp

prepeak in the experimental $S_N(k)$ of molten CuI,.[9,11,28]. More recently, Bitrian et al. [29,30,31] showed by MD simulations, that the inclusion of many body interactions due to the induced polarizations of the anions in the VR rigid ion potentials accounts for the small prepeak of molten AgI, as well as the first sharp diffraction peak of molten CuI.[32] The improvements of Bitrian et al. prompted us to introduce the polarization interactions in the VR rigid ion potentials of Stafford et al.[23] for CuCl, and carry out MD simulations of the resulting polarizable ion model (PIM) in order to gain more insight into the structure of CuCl by calculating its $S_{ab}(k)$, $S_N(k)$ and $A_X(k)$.

The layout of this paper is as follows. In Sec. II we establish the formalism to distinguish the Ashcroft-Langreth and Faber-Ziman structure factors. The methodology is described in Sec. III, where we explain the HEXRD measurement of molten CuCl and the reverse Monte Carlo technique of structural modeling, and describe the PIM for CuCl and give some details of MD simulations. We present and discuss the results in section IV, and summarize them in the concluding remarks of section V.

II. FORMALISM

The basic properties to describe the structure of polyatomic systems are the partial radial distribution functions $g_{ab}(r)$ and the Ashcroft-Langreth (AL)[33] partial structure factors $S_{ab}(k)$ related by the Fourier transform[2, 6]

$$S_{ab}(k) = \delta_{ab} + \sqrt{c_a c_b}\,\rho \int_0^\infty [g_{ab}(r) - 1] \frac{\sin kr}{kr} 4\pi r^2 dr \tag{1}$$

where δ_{ab} is the Kronecker delta and $c_a = N_a/N$ is the partial atomic number density with N_a equals the number of particles of spices a and $N = \Sigma N_\alpha$. In MD simulations, $S_{ab}(k)$ can also be evaluated directly by using

$$S_{ab}(k) = \frac{1}{\sqrt{c_a c_b}} \frac{1}{N} \langle \sum_{ia=1}^{Na} \exp(i\mathbf{k}\cdot\mathbf{r}_{ia}) \sum_{jb=1}^{Nb} \exp(-i\mathbf{k}\cdot\mathbf{r}_{jb}) \rangle \tag{2}$$

where $\mathbf{r}_{ia}$ is the position of the particle i_a of species a and the angular brackets denote the ensemble average over the equilibrium configurations. Other authors, e.g., Hansen and McDonald,[34] and McGreevy,[35] do not include the factor $(c_a c_b)^{-1/2}$ in Eq. (2), and then write $(c_a c_b)$ instead of $(c_a c_b)^{1/2}$ in Eq. (1). By using Eqs. (1) and (2), as Eisenberg et al.,[2] Rovere and Tosi,[6] and Price and Copley,[36] $S_{ab}(k)$ approaches to δ_{ab} as k goes to ∞. From the partials $S_{ab}(k)$, the coherent neutron or X-ray diffraction structure factors in the AL form are given by

$$S_D(k) = \frac{1}{f_{coh}^2} \sum_a \sum_b \bar{f}_a \bar{f}_b \sqrt{c_a c_b} S_{ab}(k) \tag{3}$$

where D refers to neutron (N) or X-ray (X) diffraction experiments, $\bar{f}_a$ can be either the neutron scattering length $\bar{b}_a$ or the wavenumber dependent atomic form factor $f_a(k)$, and $f_{coh}^2 = \Sigma c_a \bar{f}_a^2$, is the mean square value over all species, $4\pi \bar{f}_a^2$ is the coherent scattering cross section per particle of type a, so that $S_D(k)$ approaches unity as k goes to ∞.

While theoretical and simulation papers commonly use the AL structure factors, experimental data usually refers to the Faber-Ziman (FZ)[37] structure factors. The FZ diffraction structure factors are

$$A_D(k) = \frac{1}{\bar{f}^2} \sum_a \sum_b \bar{f}_a \bar{f}_b c_a c_b A_{ab}(k) = 1 + \frac{f_{coh}^2}{\bar{f}^2}[S_D(k) - 1] \tag{4}$$

where $\bar{f} = \Sigma c_a \bar{f}_a$ and the FZ partial structure factors are[6]

$$A_{ab}(k) = 1 + \frac{1}{\sqrt{c_a c_b}}[S_{ab}(k) - \delta_{ab}] \tag{5}$$

which allows $g_{ab}(r)$ to be determined by [35]

$$g_{ab}(r) = 1 + \frac{1}{\rho(2\pi)^3} \int_0^\infty [A_{ab}(k) - 1] \frac{\sin kr}{kr} 4\pi k^2 dk \tag{6}$$

Both $A_D(k)$ and $A_{ab}(k)$ also approach unity as k goes to ∞.

The differential cross section per particles can be written as[6, 38]

$$\frac{1}{N}\frac{d\sigma}{d\Omega} = f_{coh}^2 S_D(k) + (f_T^2 - f_{coh}^2) = \bar{f}^2[A_D(k) - 1] + f_T^2 = F(k) + f_T^2 \tag{7}$$

where $f_T^2 = \Sigma c_a \overline{f_a^2}$, being $4\pi \overline{f_a^2}$ the total scattering cross section per particle of type *a*, $(f_T^2 - f_{coh}^2)$ is the incoherent contribution, and $F(k) = \overline{f_a}^2 [A_D(k)-1]$ is the interference function related to the correlations between distinct particles. [39] It should be noted that $S_D(k)$ is also called the *total* structure factor because it is a combination of the partials.[2] Nevertheless, $S_D(k)$ is the coherent contribution to the *total* differential cross section and the second member in Eq. (7) is analogue to that for monoatomic systems.

III. METHODOLOGY

A. High-energy X-ray diffraction measurements and RMC structural modeling

Firstly, a powder sample of CuCl was sealed in a quartz tube under vacuum at 1073K to produce a bulk solid and to eliminate the moisture in the sample. Following this process, the bulk sample was sealed in a fused silica capillary (2.4 mm inner diameter and 0.25 mm wall thickness) for the measurement. The high-energy X-ray diffraction (HEXRD) measurement of molten CuCl at T = 773K was carried out at the BL04B2[40] in SPring-8, with the incident X-ray beam from a Si(111) monochromator, using the third harmonic reflection at an energy value of 113.4 keV and a wavelength of 0.1093 Å. Scattering intensities were measured with a Ge detector in a transmission mode. Diffraction patterns were obtained at angle intervals of 0.05º over the small-angle region from 0.3º to 5º, 0.075º over the middle-angle region from 4º to 11.5º, and 0.15º over the large-angle region from 10º to 19.9º. The accessible momentum transfer k ranged from 0.3 to 19.9 $Å^{-1}$. The resulting X-ray diffraction data were corrected for polarization, absorption, and background contributions from the capillary and the instrument, then the Compton scattering contribution was subtracted and the corrected data sets were normalized to give the Faber-Ziman structure factor $A_X(k)$.

We carried out the RMC structural modeling for molten CuCl by using RMC++ code.[41] 5000 ions (N_{Cu} = 2500 and N_{Cl} = 2500) were randomly placed in a cubic cell with periodic boundary

conditions as an initial configuration, where all ions are separated from each other over the closest inter-ionic distances r_c which are 2.0, 2.0, and 3.0 Å for Cu-Cu, Cu-Cl, and Cl-Cl pairs, respectively. We chose these values from the radial distribution functions in Ref. 4. In the RMC process, an ion is randomly moved to a new position within a max-move distance (0.25 Å) avoiding distances shorter than r_c. After moving only one ion, for each available experimental structure factor, $A_D^E(k)$ where D labels the different diffraction experiments, the corresponding structure factors $A_D^C(k)$ are calculated for the new configuration, and the difference between calculations and experiments is quantified by[41,]

$$\chi^2 = \sum_D \sum_j [A_D^C(k_j) - A_D^E(k_j)]^2 / \sigma_D^2 \tag{8}$$

where the sum is over all the experimental points j and over all available experimental structure factor D, and σ_D is the estimated experimental error, which functions as a 'control parameter' for the simulation. (By prescribing how close a fit to experimental data is required, σ_D controls the ratio of the numbers of accepted/attempted moves). If χ_n^2 for the new configuration is smaller than χ_o^2 for the old, the new configuration is accepted. If χ_n^2 is larger, the new configuration is accepted with probability exp(-(χ_n^2 - χ_o^2)/2).[43] The RMC++ program repeats these procedures until χ_n^2 is minimized. In the present study, we used the four structure factors: our $A_X(k)$, with σ_D = 0.005, the latest $S_N(k)$ reported by Drewitt et al.[11] for natural composition, with σ_D = 0.01, and both the $S_N(k)$ reported by Eisenberg et al.[11] for two different isotopic compositions, also with σ_D = 0.01. In this case, χ_n^2 is calculated on the basis of the four structure factors and the acceptance condition of the ionic movement is severer than when we use only $A_X(k)$. We set the ionic number density at 773 K as ρ = 0.041 ions/Å^3.[42] Although the $S_N(k)$ by Drewitt et al. was measured at a slightly lower temperature (733K rather than 773K for our and Eisenberg's data), we assume that this difference is small for structure factor data. Although the RMC modeling for molten CuCl has already been carried out by McGreevy and Pusztai,[4] our RMC results include new experimental information,

because our $A_X(k)$ and $S_N(k)$ reported by Drewitt et al.[11] are measured up to the high-k region. Moreover, they reported the partial $g_{ab}(r)$ but not the partial $S_{ab}(k)$.

B. Polarizable ion model and MD simulations

Using our own software, we carried out MD simulations of a rigid and a polarizable ion model for molten CuCl. The rigid ion model (RIM) is based on the ion pair potential in the VR functional form[19] which can be written as

$$\phi_{ab}(r) = \phi^0_{ab}(r) - \frac{P_{ab}}{r^4} \tag{9}$$

with

$$\phi^0_{ab}(r) = \frac{z_a z_b e^2}{r} + \frac{H_{ab}}{r^7} - \frac{C_{ab}}{r^6}\,. \tag{10}$$

The first term on the rhs of Eq. (10) is the Coulomb interaction between the charges, with z_a the effective charge in units of the fundamental charge e. lower than unity in order to rule the incomplete ionization asserted by Enderby and Neilson.[5] The second one models the repulsion between the ions with $H_{ab} = A(\sigma_a+\sigma_b)^7$, where σ_a are related to the ionic radii, with σ_{Cu} = 0.430 Å much smaller than σ_{Cl} = 1.911 Å, and A defines the strength of the repulsive interactions. And the third is the van der Waals contribution with $C_{ab} = (3/2)\alpha_a\alpha_b(E_a^{-1} + E_b^{-1})^{-1}$, where α_a are the polarizabilities and E_a are related to the ionization potentials of the cations and electron affinities of the anions. The second term on the rhs of Eq. (9) denotes the effective monopole-induced dipole interaction with $P_{ab} = (1/2)(\alpha_a z_b^2 + \alpha_b z_a^2)e^2$. Then, assuming α_{Cu} = 0, it leads to C_{CuCu} = C_{CuCl} = P_{CuCu} = 0. We used the potential parameter values proposed for molten CuCl by Stafford et al.:[23] z = 0.501, A = 0.1603 eV, σ_{Cu} = 0.430 Å, σ_{Cl} = 1.911 Å, α_{Cl} = 3.45 Å^3 and C_{ClCl} 83.1 eVÅ^6.

The polarizable ion model (PIM) is constructed by adding the many-body induced polarization interactions to the pair potential $\phi^0_{ab}(r)$. We assume that only the anions are polarizable and then, on an ion placed at position $\mathbf{r}_i$, the local electric field $\mathbf{E}_i$ due to all the other ions induces a point dipole whose moment is

$$\boldsymbol{\mu}_i = \alpha_i \mathbf{E}_i = \alpha_i (\mathbf{E}_i^{\mathrm{q}} + \mathbf{E}_i^{\mu}) , \tag{11}$$

where $\mathbf{E}_i^{\mathrm{q}}$ is the field at $\mathbf{r}_i$ due to all the point charges except $q_i = z_i e$, and $\mathbf{E}_i^{\mu}$ the field at $\mathbf{r}_i$ due to all the dipole moments except $\boldsymbol{\mu}_i$. The potential energy of this PIM can be written as

$$U = \frac{1}{2}\sum_{i=1}^{N}\sum_{j\neq i}^{N}\phi_{ij}^{0}(r_{ij}) - \sum_{i=1}^{N}\boldsymbol{\mu}_i \cdot \mathbf{E}_i^{\mathrm{q}} - \frac{1}{2}\sum_{i=1}^{N}\boldsymbol{\mu}_i \cdot \mathbf{E}_i^{\mu} + \sum_{i=1}^{N}\frac{\mu_i^2}{2\alpha_i} . \tag{12}$$

In carrying out the MD simulations, we actually have to calculate the forces. The force acting in an ion is that given in Ref. 43.

By using the RIM and PIM described above, we simulated molten CuCl at 773 K, the same temperature as the HEXRD measurements of this work and ND data of Shirakawa et al.,[9] and close to the 733 K of ND data of Drewitt *et al*.[11] The ionic density was set as 0.041 ions/Å^3,[44] which is the same as RMC modeling. MD simulations were carried out at constant energy considering N = 1000 ions placed in a cubic box of side $L = (\rho/N)^{-3}$ with periodic boundary conditions, using the Beeman's integration algorithm (see Ref. 44) with a time step of 5×10^{-15} s and, once equilibrium was achieved, the properties were averaged over 450000 time steps. The electric fields and the corresponding long-range interactions were evaluated by the Ewald method (see Ref. 44) with the Ewald parameter equal to 6.5/L. The real space terms were truncated at distances longer than L/2, and the reciprocal space contributions of wave vectors $\mathbf{k} = \mathbf{n}(2\pi/L)$, $\mathbf{n}$ being a vector of integer components, were truncated for n^2 higher than 12. The dipole moments have been evaluated by using the prediction-correction iterative method proposed by Vesely[45] with 10^{-4} as convergence limit. We adopt a hybrid method for the evaluation of $S_{ab}(k)$. For k beyond 4 Å^{-1}, we evaluated Eq. (1) up to L/2 instead of ∞. At low k this method gives spurious oscillations due to truncation errors, and therefore we computed $S_{ab}(k)$ directly, up to 4 Å^{-1} and slightly beyond, by using Eq (2). More computational details are described in Ref. 43.

IV. RESULTS AND DISCUSSION

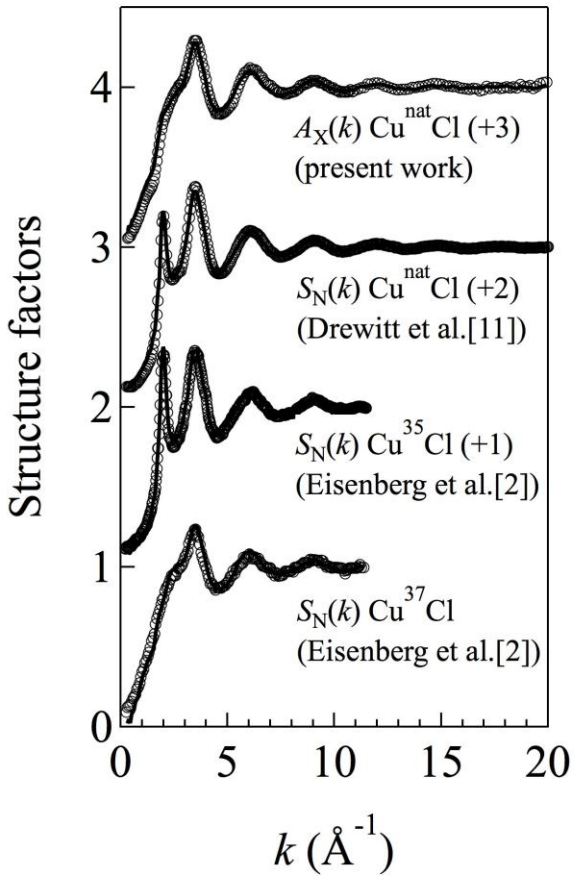

FIG. 1. Structure factors from experimental measurements (open circles) and RMC (solid line).

The X-ray diffraction structure factor $A_X(k)$ obtained in the present work is shown in Fig. 1 together with three earlier neutron diffraction structure factors $S_N(k)$ reported by Drewitt et al.[11] for natural composition of CuCl and by Eisenberg et al.[2] for two different isotopic compositions. As in the three $S_N(k)$, our $A_X(k)$ also shows clear oscillation beyond the main peak at approximately 3.4 Å^{-1}. $A_X(k)$ exhibits a shoulder at about 2.4 Å^{-1}, which is also observed in the $S_N(k)$ for $Cu^{37}Cl$, and becomes a clear peak in the $S_N(k)$ for $Cu^{35}Cl$ and $Cu^{nat}Cl$. In addition, $A_X(k)$ presents a small shoulder at approximately 1.2 Å^{-1}, which suggests intermediate-range ordering, but much less pronounced than in molten CuI and CuBr whose $S_N(k)$ by Shirakawa et al.[9] exhibit a prepeak. A similar small shoulder was also found by Shirakawa et al. (see Fig. 4) in the $S_N(k)$ for $Cu^{nat}Cl$. The RMC results reasonably reproduce the four input structure factors as shown in Fig. 1. Since the

experimental structure factors for CuCl consists of three $S_{ab}(k)$ (ab = CuCu, CuCl, ClCl) as given by Eqs. (3) and (4), three different $S(k)$ are needed to obtain the accurate $S_{ab}(k)$. In this paper we use four input $S(k)$ data for the RMC. If these input data were inconsistent with each other, the RMC algorithm would not be able to find the solution, which reproduces all the input data. However there is a good agreement between experimental and RMC data, therefore indicating that our $A_X(k)$ and the earlier three $S_N(k)$ are consistent with each other. We did not achieved the same agreement by running the RMC calculations with the Shirakawa's data in place of Drewitt's data, since the RMC results did not reproduce the shoulder at around 1 Å^{-1} observed by Shirakawa et al. We think that their measurements are not enough reliable, probably due to a bad subtraction of the scattering contribution from the silica glass container, which has a diffraction peak at around 1.5 Å^{-1}.

. Since $\bar{b}_{Cl}^2 / \bar{b}_{Cu}^2 > 1$ for Cu^{35}Cl and Cu^{nat}Cl (see Table I), the clear first peak at 2.4 Å^{-1}comes from $S_{ClCl}(k)$, whose contribution in Cu^{37}Cl is much lower because $\bar{b}_{Cl}^2 / \bar{b}_{Cu}^2 = 0.18$. In fact, this clear first peak is due to the main peak of $S_{ClCl}(k)$, which is much higher than that for the structure-less $S_{CuCu}(k)$ as is shown by the $S_{ab}(k)$ determined by Eisenberg et al.,[2] as well as the partials reported in this work (see below). Our $A_X(k)$ resembles very much the $S_N(k)$ for Cu^{37}Cl because of the mean value $f_{Cl}^2 / f_{Cu}^2 \approx 0.32$ (see Table II) is also lower than 1.

TABLE 1: Neutron scattering lengths, $\bar{b}_a$ in fm,[46]

	Cu	^{nat}Cl	^{35}Cl	^{37}Cl
$\bar{b}_a$	7.718	9.577	11.65	3.08
$\bar{b}_{Cl}^2 / \bar{b}_{Cu}^2$		1.54	2.23	0.18

TABLE II: X-ray form factors $f_a(k)$ in electrons,[47] and the mean value f_m from 1.0 to 3.5 Å^{-1}

	Cu	Cl	f_{Cl}^2 / f_{Cu}^2
f_a (1.2 Å^{-1})	26.8	15.8	0.35
f_a (2.4 Å^{-1})	23.9	12.3	0.26
f_a (3.4 Å^{-1})	21.0	10.1	0.23
f_m	25.5	14.3	0.32

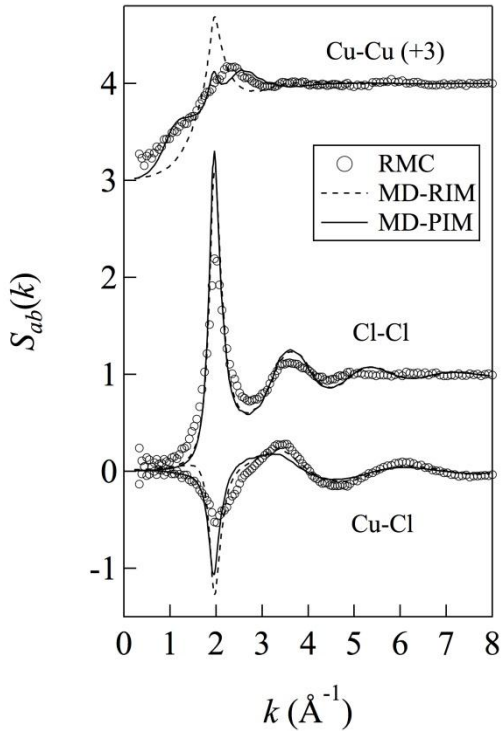

FIG. 2. $S_{ab}(k)$ from RMC (open circles) and MD simulations of RIM (dashed line) and PIM (solid line).

The partial AL structure factors $S_{ab}(k)$ from RMC modeling of our $S_X(k)$, are shown in Fig. 2 together with those from PIM and RIM simulations. The RMC $S_{CuCu}(k)$ shows a maximum at around 2.2 Å^{-1}, which is slightly shifted from that reported by Eisenberg et al.[2] at about 2.0 Å^{-1}, and its structure-less features at higher k are similar to those by Eisenberg et al. The PIM $S_{CuCu}(k)$ is very similar to the RMC result in comparison with the RIM result. The height of the peaks is almost the same, while that for RIM is clearly higher. Moreover, the PIM $S_{CuCu}(k)$ reproduces the shoulder in the vicinity of 1.2 Å^{-1}, which indicates intermediate-range ordering of Cu ions due to the anion polarization effects. The structural origin of this shoulder is probably related to the length scale that characterizes the ordering of the voids between cations as was shown for molten AgI and CuI.[29,32] Hence, the PIM $S_{CuCu}(k)$ demonstrates that the anion polarization is essential to explain the molten CuCl structure. The three $S_{ClCl}(k)$ in Fig. 2 exhibit a sharp main peak at approximately 2.0 Å^{-1}, higher for MD results, and larger oscillations than $S_{CuCu}(k)$ at longer k, showing that the Cl anions are closely packed because of their large size in comparison with the Cu cations. Both RIM and

PIM $S_{ClCl}(k)$ are very similar, indicating that the anion polarization effects are very small in the anion structure but not in the smaller cations, as it was already observed from MD simulations of molten AgI and CuI using PIM.[29,32] The RMC $S_{CuCl}(k)$ shows the first valley at approximately 2.0 $Å^{-1}$, which is well reproduced by MD simulations, although those from MD are deeper. The first peak of the $S_{CuCl}(k)$ at about 3.4 $Å^{-1}$ is located at almost the same-position of the second peak of $S_{ClCl}(k)$, which largely contributes to the main peak of $S_X(k)$.

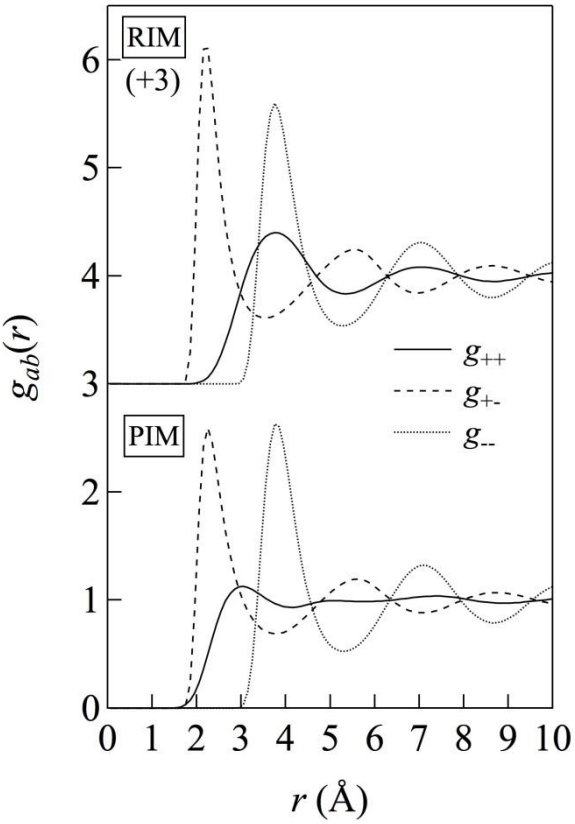

FIG. 3. $g_{CuCu}(r)$ (solid line), $g_{CuCl}(r)$ (dotted line), and $g_{ClCl}(r)$ (dashed line), from MD simulations of RIM (upper panel) and PIM (bottom panel).

The partial radial distribution functions $g_{ab}(r)$ from RIM and PIM simulations are shown in Fig. 3. As was expected from the partial structure factors in Fig. 2, the differences between the anion correlations for RIM and PIM are very small, and confirm that the induced polarization in the Cl ions practically does not affect their closely packed structure. Correlations between unlike ions are also similar, with the first peak of the PIM $g_{CuCl}(r)$ lower than that for RIM. The most salient differences between RIM and PIM are found in the cation correlations. At first glance, the $g_{CuCu}(r)$

determined by Eisenberg et al.[2] resembles more the PIM result than the RIM. The PIM $g_{CuCu}(r)$ is neither in phase with $g_{ClCl}(r)$ nor in opposite phase with $g_{CuCl}(r)$, as it is in the RIM case and the typical structure of molten alkali halides. While the RIM $g_{CuCu}(r)$ has its maximum at the same position as that of $g_{ClCl}(r)$, the maximum of the PIM $g_{CuCu}(r)$ is shifted inwards with a deeper penetration of the small cations into the first coordination shell of unlike ions. This feature, which has also been observed from MD simulations of molten AgI and CuI using PIM,[29,32] is attributed to the screening of the cations repulsion due to the anion-induced dipoles, i.e. the negative ends of the anion dipoles attract the cations. Furthermore, the PIM $g_{CuCu}(r)$ presents a second small maximum before the second peak of $g_{CuI}(r)$. The picture that emerges from the two maxima of $g_{CuCu}(r)$ between the two peaks of $g_{CuI}(r)$ is that around each copper cation there is a double shell of cations between the first and second shells of chlorides. Therefore, at larger distances, the weak oscillations in g_{CuCu}(r) do not repeat themselves with a clear wavelength. This is the reason why $S_{CuCu}(k)$ exhibits a double maxima at around 2.2 $Å^{-1}$.

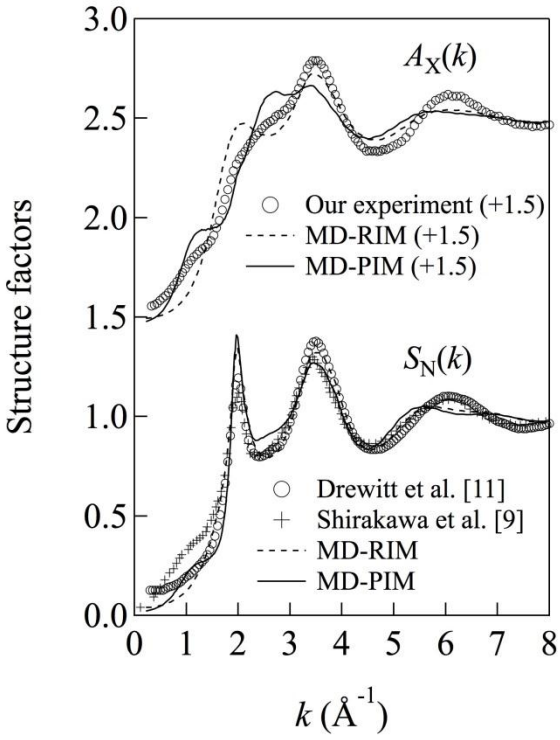

Fig. 4. Structure factors from experimental measurements (open circles or crosses) and MD simulations of RIM (dashed line) and PIM (solid line).

In Fig. 4, a comparison is made between experimental and MD structure factors. The PIM $A_X(k)$ has the main peak at approximately 3.3 Å^{-1}, which is almost at the same position as the X-ray result, although it is slightly lower than the experimental one. This peak comes from the second maxima of $S_{ClCl}(k)$ and the first one of $S_{ClCu}(k)$. A large shoulder, or even a peak, is found in the PIM $A_X(k)$ at around 2.6 Å^{-1}, which is higher and at a longer position than that for both RIM and the experimental results at 2.4 Å^{-1}. Since $f_{Cl}^2 / f_{Cu}^2 \approx 0.32$, these shoulders, and their discrepancies, result in a delicate balance between the positive contribution of the weighted down first peak of $S_{ClCl}(k)$ and the negative contribution of the also weighted down first valley of $S_{ClCu}(k)$, together with the small contributions of $S_{CuCu}(k)$. However, the small shoulder in the experimental $A_X(k)$ at 1.2 Å^{-1}, which comes from the shoulder of $S_{CuCu}(k)$, is reasonably reproduced by the PIM, but not by the RIM.

The position and height of the two main peaks of the experimental $S_N(k)$ for $Cu^{nat}Cl$ are well reproduced by RIM and PIM, although the oscillations beyond the peaks in MD results are more damped with a slightly different periodicity. Now, since $\bar{b}_{Cl}^2 / \bar{b}_{Cu}^2 = 1.54$, the first peak of $S_{ClCl}(k)$ is weighted high and it is clearly observed in $S_N(k)$. The PIM $S_N(k)$ shows a small shoulder in the vicinity of 1.2 Å^{-1} similar to that of the $S_N(k)$ by Shirakawa et al.[9] (whose values are higher), which is neither found in the $S_N(k)$ by Drewitt et al.[11] nor in the RIM case. This difference does not contradict the importance of the anion polarization effect because it is necessary to reproduce $S_{CuCu}(k)$ obtained by experimental analyses, whose contribution to the $S_N(k)$ for $Cu^{nat}Cl$ is very small.

V. CONCLUDING REMARKS

We carried out high-energy X-ray diffraction (HEXRD) measurements of the structure factor $A_X(k)$ of molten CuCl at 773 K, and the reverse Monte Carlo (RMC) modeling method shows that it is consistent with the earlier neutron diffraction (ND) structure factors $S_N(k)$ reported by other authors.[2,9,11] Moreover, we also carried out molecular dynamics (MD) simulations of molten CuCl

using both a rigid and a polarizable ion model. The rigid ion model (RIM) is based on the ion pair potential of the Vashishta and Rahman functional form,[19] in which the cations are much smaller than the anions. The polarizable ion model (PIM) is based on the RIM but assuming that the chloride anions are polarizable and adding the corresponding many-body induced polarization interactions.

The PIM simulated structure factors reproduce all trends observed experimentally. To our knowledge, this is the first time since the pioneering works of 1971 that the structural features of molten CuCl are reproduced and explained from a theoretical model. The differences between the Cl-Cl correlations for RIM and PIM are very small because the induced polarization in the Cl ions practically does not affect their closely packed structure. The main difference between both models are found in the Cu-Cu correlations with the much less structured PIM $S_{CuCu}(k)$ being more similar to that obtained from RMC modeling of experimental data. This result shows that the anion polarization effects are necessary for a better reproduction of the overall structure of molten CuCl, in particular the small shoulder at around 1 Å as a signature of some intermediate-range ordering. Nevertheless, this polarization effect in molten CuCl is less important than in molten CuI and AgI because the chloride polarizability (3.46 Å^3) is lower than the iodide one (≈ 6 Å^3). Furthermore, since $\bar{b}_I$ = 5.280 fm, and thus $\bar{b}_{Cu}^2 / \bar{b}_I^2$ = 2.13, the $S_{CuCu}(k)$ contribution to the $S_N(k)$ for CuI is very high and $S_N(k)$ exhibits a clear prepeak.[9,11,32] In molten AgI, since $\bar{b}_{Ag}$ = 5.922 fm, and thus $\bar{b}_{Ag}^2 / \bar{b}_I^2$ = 1.14, its $S_N(k)$ only presents a small maximum.[10,29] In CuCl, because of the lower chloride polarizability and because of $\bar{b}_{Cu}^2 / \bar{b}_{Cl}^2$ = 0.65, the small shoulder can hardly be distinguished in its $S_N(k)$, but it can be appreciated in its $A_X(k)$ because of f_{Cu}^2 / f_{Cl}^2 ≈ 3.13.

While solid AgI and CuI, as well as CuBr, undergo a first order structural β-α phase transition before melting and become superionic, CuCl melts from β-phase. Why CuCl does not possess a true superionic phase, is an important issue to pursue further because it would help to understand better the mechanism of rapid ionic diffusion in solids. In the high temperature superionic α-phase, AgI

and CuI form a body centered cubic (bcc) and a face centered cubic (fcc) lattice, respectively, and cations, much smaller than anions, diffuse easily through it.[12,48] This behavior was account by MD simulations using rigid ion VR potentials and, more recently, by using a polarizable ion model. The later shows that the averaged spatial distribution of the cations caused by the polarized iodides is in better agreement with experimental studies, which conclude that the diffusive motion of silver ions consists of jumps between adjacent tetrahedral sites via trigonal sites, with a small occupation of octahedral sites.[48] These results show that the ionic size difference effects are crucial in the superionic behavior, while polarization effects are necessary for a better reproduction of this phenomenon. On the other hand, at the high temperature β-phase, CuCl presents a wurtzite structure, where copper cations form a hexagonal close-packed (hcp) lattice shifted vertically from the hcp lattice of chlorides, and the ionic conductivity increases with temperature up to about 0.1 $(\Omega cm)^{-1}$ before melting without any first order structural phase transition.[15.48] As for AgCl and AgBr, the ionic conductivity is due to the cationic Frenkel defects, and it is suggested that a possible diffuse transition to a superionic state is frustrated by the disordering of the anionic sublattice due to Schottky defects which leads to melting.[49, 50] This behavior may be because the size difference between cations and anions in CuCl is less pronounced than in AgI and CuI, and also because the chloride polarizability s lower than the iodide one. To answer this question would be necessary to carry out MD simulations of CuCl before melting using non-cubic boundary conditions, which are not available in our own programs, as it is the case in many standard MD simulation software.

ACKNOWLEDGMENTS

O. Alcaraz and J. Trullas thank Generalitat de Catalunya for Grant No. 2009SGR-1003 and MINECO of Spain for Grant No. FIS20012-39443-C02-01. The synchrotron radiation experiments were performed at the BL04B2 at SPring-8 with the approval of the JASRI (Proposal No. 2005A0711).

[1]D. I. Page and I. Mika, J. Phys. C: Solid State Phys. 4, 3034 (1971).

[2]S. Eisenberg, S. F. Jal, J. Dupuy, O. Chieux, and W. Knoll, Phil. Mag. A **46**, 195 (1982).

[3]R. L. McGreevy, J. Phys. Condens. Matter **13**, R877 (2001).

[4]R. L. McGreevy and L. Pusztai, Proc. R. Soc. Lond. A **430**, 241 (1990).

[5]J. E. Enderby and G. W. Neilson, Adv. Phys. **29**, 323 (1980).

[6]M. Rovere and M. P. Tosi, Rep. Prog. Phys. **49**, 1001 (1986).

[7]L. V. Woodcock, *Chem. Phys. Let.* **10**, 257 (1971).

[8]F. G. Edwards, J. E. Enderby, R.A. Howe, and D. I. Page, J. Phys. C **8** 3483 (1975); E. W. J. Mitchell, P. F. J. Poncet, and R. J. Stewart, Phil. Mag. **34**, 721 (1976); J. Y. Derrien and J. Dupuy, J. de Phys. **36**, 191(1975); J. Locke, S. Messoloras, R. J. Stewart, R. L. McGreevy, and E. W. J. Mitchell, Phil. Mag. B **51** 301 (1985); M. A. Howe, R. L. McGreevy, and W. S. Howells, J. Phys.: Condens. Matter **1**, 3433 (1989).

[9]Y. Shirakawa, M. Saito, S. Tamaki, M. Inui, and S. Takeda, J. Phys. Soc. Jpn. **60**, 2678 (1991).

[10]M. Inui, S. Takeda, Y. Shirakawa, S. Tamaki, Y. Waseda, and Y. Yamaguchi. J. Phys. Soc. Jpn. **60**, 3025 (1991); Y. Shirakawa, S. Tamaki, T. Usuky, K. Sugiyama, and Y. Waseda, J. Phys. Soc. Jpn. **63**, 1814 (1994); Y. Kawakita, S. Tahara, H. Fujii, S. Kohara and S. Takeda, J. Phys.: Condens. Matter **19**, 335201 (2007); Y. Kawakita, T Enosaki, S. Takeda, and K. Maruyama, J. Non-Cryst. Solids **353**, 3035 (2007).

[11]J. W. E. Drewitt, P. S. Salmon, S. Takeda, and Y. Kawakita, J. Phys.: Condens. Matter **21**, 075104 (2009).

[12]M. A. Howe, R. L. McGreevy, and E. W. J, Mitchell, Z. Phys. B **62**, 15 (1985).

[13]M. Ginoza, J. H. Nixon, and M. Silbert, J. Phys. C: Solid State Phys. **20**, 1005 (1987).

[14]J. B. Boyce and B. A. Huberman, Phys. Rep. **51**, 189 (1979).

[15]S. Hull, Rep. Progr. Phys. **67**, 123 (2004).

[16]D. A. Allen and R. A. Howe, J. Phys. Condens. Matter **4**, 6029 (1992).

[17]Y. Waseda, S. Kang, K. Sigiyama, M. Kimura, and M. Saito, J. Phys. Condens. Matter **12**, A195 (2000).

[18]P. Vashishta and A. Rahman, Phys. Rev. Lett. **40**, 1337 (1978).

[19]P. Vashishta and A. Rahman, *Fast Ion Transport in Solids*, ed. P. Vashishta; J. N. Mundy, and G. K. Shenoy, North-Holland, Amsterdam, 1979.

[20]M. Parrinello, A. Rahman, and P. Vashishta, Phys. Rev. Lett. **50**, 1073 (1983).

[21]J. L. Tallon, Phys. Rev. B **38**, 9069 (1988); K. O'Sullivan, G. Chiatotti, and P. A. Madden, Phys. Rev. B **43**, 13536 (1991); P. A. Madden, K. O'Sullivan, and G. Chiatotti, Phys. Rev. B **45**, 10206 (1992); C. Seok and D. W. Oxtoby, Phys. Rev. B **56**, 11485 (1997); Ibid **58**, 5146 (1998); D. A. Keen, S. Hull, A. C. Barnes, P. Berastegui, W. A. Crichton, P. A. Madden, M. G. Tucker, and M. Wilson, Phys. Rev. B, **68**, 014117 (2003).

[22]A. Chaid and R. L. McGreevy, J. Phys.: Condens. Matter **10**, 2597 (1998); J. X. M. Zheng-Johansson, I. Ebbsjö, and R. L. McGreevy, Solid State Ionics **82**, 115 (1995); J. X. M. Zheng-Johansson and R. L. McGreevy, Solid State Ionics **83**, 35 (1996); J. X. M. Zheng-Johansson, R. L. McGreevy, and I. Ebbsjö, Physica B **226**, 107 (1996); R. L. McGreevy and J. X. M. Zheng-Johansson, Solid State Ionics **95**, 215 (1997).

[23]A. J. Stafford and M. Silbert, Z. Phys. B **67**, 31 (1987).

[24]A. J. Stafford, M. Silbert, J. Trullas, and A. Giró, J. Phys.: Condens. Matter **2**, 6631 (1990). In this article, the curves should be interchanged between figures 2 and 3 in order to match the figure captions. Moreover, in Table 1 the value of α_X for AgI should be 6.52 Å^3 and that of H_{XX} for CuI should be 399 in energy units of $e2$/Å = 14.4 eV as in Ref. 19.

[25]H. Takahashi, S. Takeda, S. Harada, and S. Tamaki, J. Phys. Soc. Jpn. 57, 562 (1988).

[26]J. Trullas, A. Giró, and M. Silbert, J. Phys.: Condens. Matter **2**, 6643 (1990).

[27]V. Bitrian, J. Trullas, M. Silbert, T. Enosaki, Y. Kawakita, and S. Takeda, J. Chem. Phys. **125**, 184510 (2006).

[28]S. Takeda, H. Fujii, Y. Kawakita, Y. Kato, S. Kohara, and K. Maruyama, Physica B **385–386**, 249 (2006).

[29]V. Bitrian, J. Trullas, M. Silbert, J. Chem. Phys. **126**, 021105 (2007);

[30]V. Bitrian and J. Trullas, J. Phys. Chem. B **112**, 1718 (2008);

[31]V. Bitrian and J. Trullas, J. Phys.: Conf. Series **98**, 042006 (2008); V. Bitrian, O. Alcaraz, and J. Trullas, J. Chem. Phys. **130**, 234504 (2009).

[32]V. Bitrian, O. Alcaraz, and J. Trullas, J. Chem. Phys. **134**, 044501 (2011).

[33]N. W Ashcroft and D. C. Langreth, Phys. Rev. **156**, 685 (1967).

[34]J. P. Hansen and I. McDonald, Theory of Simple Liquids (Academic Press, London, 2006).

[35]R. L. McGreevy, Solid State Phys. **40**, 247 (1987).

[36]D. L. Price and J. R. D. Copley, Phys. Rev. A **11**, 2124 (1975).

[37]T. E. Faber and J. M. Ziman, Philos. Mag. **11**, 153 (1965).

[38]V. M. Nield and D. A. Keen, Diffuse Neutron Scattering from Crystalline Materials (Clarendon Press, Oxford, 2001).

[39]H. E Fischer, A. C Barnes, and P. S Salmon, Rep. Prog. Phys. **69** 233–299 (2006)

[40]S. Kohara, M. Itou, K. Suzuya, Y. Inamura, Y. Sakurai, Y. Ohishi, and M.Takata, J. Phys.: Condens. Matter **19**, 506101 (2007).

[41]O. Gereben, P. Jóvári, L. Temleitner and L. Pusztai, J. Optoelectron. Adv. Mater. **9**, 3021 (2007).

[42]G. J. Janz, F. W. Dampier, G. R. Lakshminarayanan, P. K. Lorenz, and R. P. T. Tomkins, Molten Salts: Volume 1. Electrical Conductance, Density, and Viscosity Data (National Standard Reference Data Series - National Bureau of Standards 15, U.S. Government Printing Office, Washington, D.C., 1968).

[43]J. Trullas, O. Alcaraz, L. E. González, and M. Silbert, J. Phys. Chem. B **107**, 282 (2003).

[44]M. J. L. Sangster and M. Dixon, Adv. Phys. **25**, 247 (1976).

[45]F. J. Vesely, J. Comput. Phys. **24**, 361 (1977).

[46]V. F. Sears, Neutron News **3**, 26 (1992). http://www.ncnr.nist.gov/resources/n-lengths

[47]P. A. Doyle and P. S. Turner, Acta Cryst. A **24**, 390-397 (1968).

[48]D. A. Keen, J. Phys.: Condens. Matter **14**, R819 (2002).

[49]W. Andreoni and M. P. Tosi, Solid State Ionics **11**, 49 (1983).

[50]M. Nield, D. A. Keen, W. Hayes, and R. L. McGreevy, J. Phys.: Condens. Matter 4, 6703 (1992).